7th Australian Conference on Laser Diagnostics in Fluid Mechanics and Combustion
Melbourne, Australia
9-11 December 2015

Effects of Nozzle Lip Thickness on the Global Modes of an Impinging Supersonic Jet

J. Weightman[1] O. Amili[1] D. Honnery[1,a] D. Edgington-Mitchell[1,a] and J. Soria[1,a,ϕ]

[1]Department of Mechanical and Aerospace Engineering, Monash University, Australia

[a]Laboratory for Turbulence Research in Aerospace and Combustion, Monash University, Australia

[ϕ]Department of Aeronautical Engineering, King Abdulaziz University, Saudi Arabia.

Abstract

Impinging jets from a thin and infinite lipped nozzle at a Nozzle Pressure Ratio (NPR) of 3.4 and plate spacing of 5.0D are investigated. The dominant modes of the jets are studied using particle image velocimetry. First and second order statistics are generated for each flow to allow for a basic comparison. A peak in transverse variance at the shock cell locations is noted for the thin lip nozzle, but not for the infinite lip case. This is associated with the existence of a global asymmetric mode for the thin lip jet and an axisymmetric mode for the infinite lip nozzle. For the infinite lip jet, this correlates with a large region of high axial variance present at the standoff shock, which is indicative of an axisymmetric mode. This difference in modes is confirmed through proper orthogonal decomposition, which shows a dominant symmetric mode for the thin lip jet and an asymmetric mode for the infinite lip case. Using the high specific energy POD modes, triple decomposition is performed on the jet flows, allowing each high variance region to be associated with its respective dominant global mode for each of the jets.

Introduction

The impingement of a jet upon a surface is a common flow condition. Research has focused on such flows due to its application to missile and rocket launching systems, VTOL aircraft and the cold spray manufacturing process. Effects of jet impingement range from ground surface erosion to lift loss and fatigue damage [10]. Impinging jets are characterized by complex shock structures [8] and production of intense discrete acoustic tones [22]. The jet structures are largely dependent on the nozzle pressure ratio (NPR), plate spacing (z/D) [11], lip thickness [24] and the impingement surface geometry [4, 18]. A schematic of these flow structures, along with an instantaneous schlieren image, is presented in Figure 1 [20].

Instabilities in the jet structure are a common phenomena in impinging jets. These instabilities are cyclic [22], with the oscillation of shock structures varying with NPR and plate spacing [10], as well as surface geometry [18]. The oscillations are dependent on the dominant global mode of the jet. This mode can be either symmetric (toroidal) or asymmetric (flapping or helical) [22]. The global mode can switch with a change in flow conditions, which changes the discrete tone frequency produced by the impinging jet [15]. The general flow structures of an impinging jet on a flat plate have been studied in depth [9, 12, 14, 16], but more work is required to understand the feedback mechanism.

Marsh [17] first noted the production of discrete tones, termed impingement tones, of a subsonic impinging jet. A feedback loop was suggested as the explanation for the production of these impingement tones [12]. This feedback loop consisted

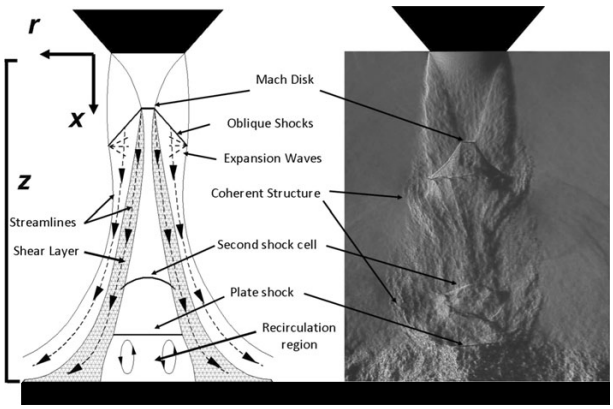

Figure 1: *General schematic and instantaneous schlieren image of an impinging flow, with key features labeled.*

of two components; the upstream propagating acoustic waves and the downstream traveling coherent structures [28]. The acoustic waves are produced at the impingement surface and travel upstream to perturb the near-exit shear layer. These small perturbations grow into large scale vortices as they travel downstream [2]. The coherent structures then interact with the plate surface, creating new acoustic waves [9, 12].

Henderson [11] used particle image velocimetry (PIV) to measure the wall jet of a supersonic impinging flow. It was suggested that a periodic coalescence of expansion regions near the impingement surface caused an oscillation in the wall jet mass flow. This led to the hypothesis that the change in mass flow causes a rapid growth of the wall jet thickness. The boundary of the wall jet acts like a membrane, creating a pressure wave as it oscillates. This pressure wave propagates upstream to the nozzle lip as an acoustic wave, closing the feedback loop. The acoustic production was observed to occur at the impingement surface, approximately 1.3 nozzle diameters from the jet centreline.

Studies of impingement geometry have shown that small, yet non-negligible, changes in peak tone frequency occur when the impingement surface is changed [22]. In addition, the sound pressure level (SPL) varies significantly due to different impingement surfaces. Mason-Smith *et al*. [18] showed that concave surface curvature is capable of stopping impingement tone production. It was also observed that the convex cylindrical sections results in a stationary flapping mode, with the flapping plane aligned along the length of the cylinder.

For free jets, Raman [24] showed that increasing the nozzle lip thickness from 0.2 to 1.0 exit diameters results in an increase

in SPL. Additionally, when the jet is highly underexpanded, upstream propagating acoustic waves can be blocked by the jet boundary removing the feedback to the nozzle lip. Increasing the lip thickness reintroduces the feedback mechanism [23]. Both free and impinging jet feedback loops are driven by the initial shear layer perturbation, and so nozzle thickness is expected to be a important parameter for impinging jets as well.

PIV was used in the recent work by Edgington-Mitchell *et al*. [7] to study the differences between a free and impinging jet at an NPR of 3.4. POD was employed to determine and compare the dominant modes of each jet. It was found that the dominant asymmetric modes of the free jet became symmetric for the impingement condition. POD was also utilized by Edgington-Mitchell et al. [5, 6] in a free jet study to observe the dominant modes and their relation to screech production. A triple decomposition method [13] was then applied to separate the coherent and stochastic fluctuations, where the coherent component was determined via the most energetic POD modes.

The effect of two nozzle designs (a thin and infinite lip nozzle) was investigated by utilizing high resolution PIV imaging. Using a sample count of over 10,000 velocity fields for each case, first and second order statistics were calculated and differences in jet structure between the two impinging flows investigated. Proper Orthogonal Decomposition is employed to separate the dominant fluctuations, allowing for comparison of the global modes of the two nozzle flow conditions.

Experimental Method

A schematic of the LTRAC supersonic jet facility is presented in Figure 2. An air line from the university compressor supplies the jet with high pressure air. The stagnation pressure was measured in the plenum chamber using an RS-461 pressure transducer. This has a range of 0-10 bar and an accuracy of $\pm 0.25\%$. The flow was seeded using a ViCount 1300 smoke generator, which produces particles approximately 600 nm in diameter. The seeded flow and air supply were injected separately into the first section of the plenum chamber. The mixed flow is then passed through a series of meshes of monotonically decreasing cell size to break up any large vortices before exiting via the nozzle.

A 15 mm diameter (D) converging nozzle, with a lip thickness of 1.5 mm, was used as the base nozzle for the experiment. A large cap, with a diameter of 15D was produced to fit atop the base nozzle. This allowed for comparison between a thin lip and an effectively infinite lip nozzle. The latter will be referred to as the infinite lip case. A schematic of both nozzles is given in Figure 3.

Single exposure image pairs were acquired using a 12-bit Imperx B6640 camera with a CCD array of 6600x4400 px. A magnification of 0.46 was achieved using a 200 mm Micro-Nikkor lens, with a Nikon PK-12 extension ring. The particle field was illuminated using a diverging light sheet of approximately 1 mm thickness produced from a dual cavity pulsed Nd:YAG laser at 532 nm, with a maximum pulse energy of 200 mJ. The pulse timing, Δt, was 884 ns. The pertinent PIV parameters are summarised in Table 1.

The multigrid cross-correlation algorithm of Soria [27] was

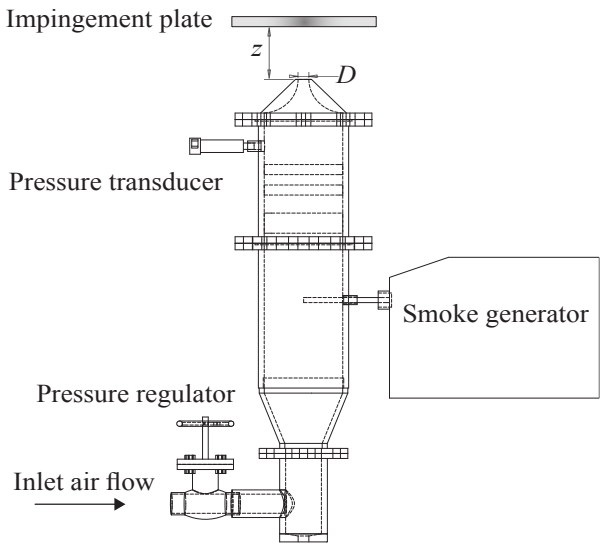

Figure 2: *Schematic of the LTRAC supersonic jet facility.*

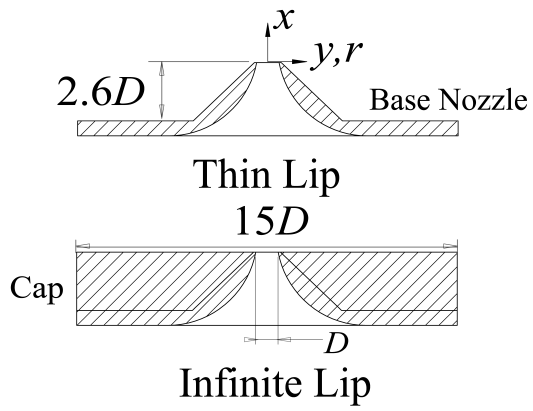

Figure 3: *Schematic of the thin and infinite lip nozzles used in the experiment.*

used to analyze the particle images. As a result of the high speed flow and high magnification present in the experiment, particle displacements between image pairs were found to be as large as 45 px. Conversely, the entrainment field often experiences single digit particle displacements. It is with this large displacement range that the multigrid algorithm is particularly useful. Thus an initial window size, IW_0, of 192x192 px and a final window size, IW_1, of 24x24 px was selected for the PIV processing.

Table 1: PIV Parameters

Parameter	Value	Non-Dimensional Value
IW_0	192	0.151D
IW_1	24	0.019D
Vector Spacing	6	0.005D
Depth of Field	0.55mm	0.037D
Field of View	78mm x 40mm	5.2D x 2.7D

Proper Orthogonal Decomposition [19, 26] was utilized to determine the dominant mode fluctuations of the flow. POD con-

structs a set of basis functions that optimally represent the ensemble of fluctuating velocities. The decomposed modes are orthogonal and ranked by energy content. Thus, the first, most energetic, modes can be associated with the coherent fluctuations that dominate the flow. This allows for the application of the triple decomposition [13], separating the flow into mean, and coherent and random fluctuating components, as given by Equation 1.

$$u_i(x,t) = U_i(x) + u_i^c(x,t) + u_i''(x,t) \tag{1}$$

where u_i is the velocity of the total flow, U_i is the mean velocity, u_i^c is the coherent velocity fluctuations and u_i'' is the random velocity fluctuations, all in the ith direction, where $i = x, y$ for Cartesian coordinates or $i = x, r$ for cylindrical coordinates.

Results and Discussion

PIV Flow Statistics

Figure 4 shows the first and second order statistics for the thin and infinite lip cases. The velocities are non-dimensionalized by the choked exit velocity,U_E, of $310m/s$. The contour maps of the first and second order statistics are obtained from over 10,000 PIV velocity vector fields. Figure 4a and 4e show the mean axial velocity for the thin and infinite lip cases, respectively. The initial expansion of the jets appear similar, reaching a maximum mean velocity of $1.8U_E$ before the first shock. In both cases, the mean wall flow is observed to approach a maximum transverse velocity of $\pm 1.1U_E$, as shown in Figure 4b and 4f. Both the thin and infinite lip flows are observed to contain four shock cells including the standoff shock. This is highlighted by the respective centreline velocities presented in Figure 5, where a sudden decrease in velocity indicates the presence of a shock.

The variances of the axial and transverse fluctuations are given in Figures 4c and 4d for the thin lip nozzle, and Figures 4g and 4h for the infinite lip nozzle. The infinite lip nozzle is observed to have the larger region of high variance at the shear layer, both axially and transversely. This is most noticeable downstream of the second shock cell. The shear layer thickness can be inferred from the axial and transverse fluctuations of the jet flow. Thus, these statistics suggest that the infinite lip nozzle has a larger shear layer than the thin lip configuration.

An increased growth rate of the coherent structures may explain the thicker shear layer observed for the infinite lip condition [2]. It may also be caused by a notable difference in entrainment field. For the infinite lip nozzle, due to the large cap, the entrainment streamlines approach the jet almost perpendicular to the bulk flow. This differs to the almost diagonal approach of the entrainment streamlines of the thin jet, as shown in Figure 6.

A high level of transverse variance is observed at the shock cell locations for the thin lip nozzle. This suggests transverse oscillation of the shock cells, which may be due asymmetric passing of shear layer vortical structures. It would thus be a result of a dominant global asymmetric mode for the thin lip configuration. Interestingly, no significant transverse variance is present at the shocks for the infinite lip case. If the high variance found in the thin lip case does correspond to an asymmetric mode, the lack of variance at the shock cells may suggest a symmetric mode for the infinite lip nozzle.

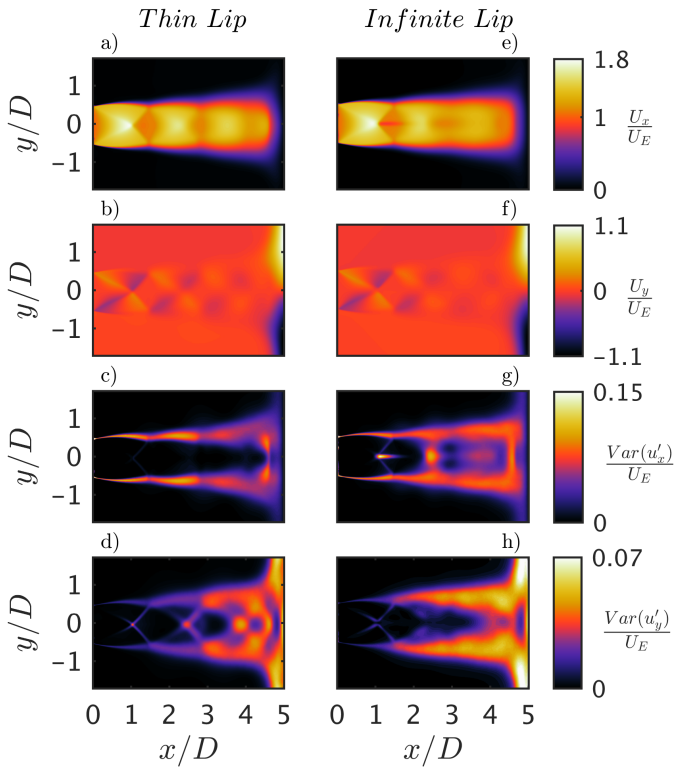

Figure 4: *a) Mean axial velocity, b) mean transverse velocity, c) variance of axial fluctuations, d) variance of transverse fluctuations for the thin lip jet. e-h are the same statistics for the infinite lip case. Statistics calculated from over 10000 samples for both cases. Flow is at an NPR = 3.4 and z/D = 5.0.*

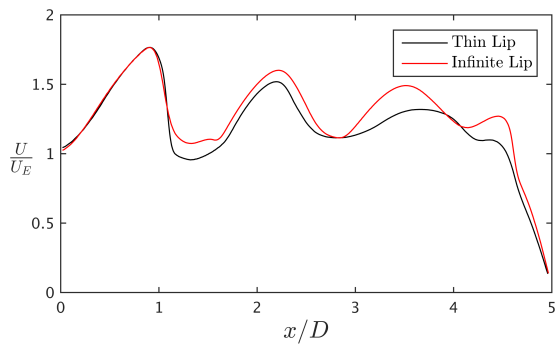

Figure 5: *Centreline velocity of both jet conditions, illustrating the existence of four shock cells in both jets. The thin lip is the upper line at $x/D = 2$.*

Similarly, of interest is the variance of the axial fluctuations at the standoff shock shown in Figures 4c and 4g. The thin lip nozzle experiences a small region of high axial variance at the standoff shock. The infinite lip configuration, however, shows an axially large region of high variance at the standoff shock. This would suggest a large axial oscillation of the standoff shock for the infinite lip case, which, as shown by Powell [22], is due to the symmetric passing of vortical structures in the shear layer. This difference in variance may show that the infinite lip jet is dominated by a global axisymmetric mode.

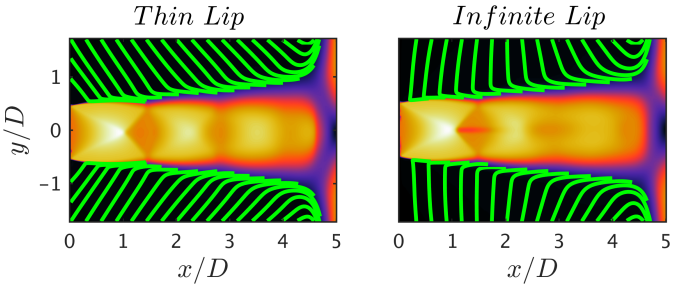

Figure 6: *Streamlines of the entrainment field flow for the thin (left) and infinite (right) lip jet. The streamlines are overlayed on the mean velocity magnitude for each configuration.*

Proper Orthogonal Decomposition

Proper orthogonal decomposition was performed on both the thin and infinite lip cases. Figure 7 shows the energy spectra of each case, which indicates the existence of one dominant mode pair for the thin lip nozzle. These modes contain 17.4% and 15.8% of the specific energy of the flow. As the flow is compressible, and density is unknown, specific kinetic energy must be used. The third mode of the POD contains only 4.1% of the kinetic energy, and is not accompanied by a modal pair. This mode has been omitted from the following figures.

Figure 8 illustrates the dominant modes of the proper orthogonal decomposition for the thin lip nozzle. Here, each mode has been individually normalized by its minimum and maximum value. From Figure 8, the structures of the first two modes are similar, but out of phase. This suggests that these modes are a modal pair that contains 33.2% of the specific kinetic energy. An observed centreline asymmetry of the axial component and symmetry of the transverse component of the POD modes exist. This suggests the flow for the thin lip nozzle is dominated by a global asymmetric mode. As the flow and impingement surface are axisymmetric, a flapping mode would most likely precess, resulting in POD modes that gradually decay in energy. As only one high energy mode pair exists and modes four and onwards contain less than 2% of the specific kinetic energy, the asymmetric mode is assumed to be helical.

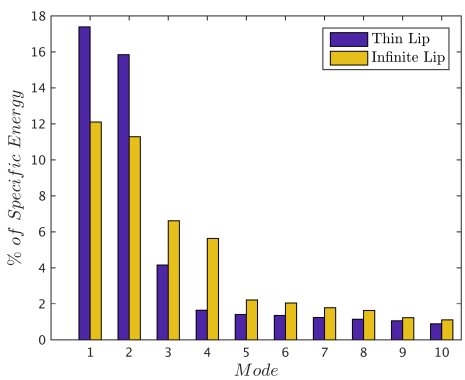

Figure 7: *Specific energy of the first 10 orthogonal modes for the thin and infinite lip cases.*

For the infinite lip condition, Figure 7 shows four dominant POD modes. The first four modes contain 12.1%, 11.3%, 6.6% and 5.6% of the specific kinetic energy, respectively. Based on

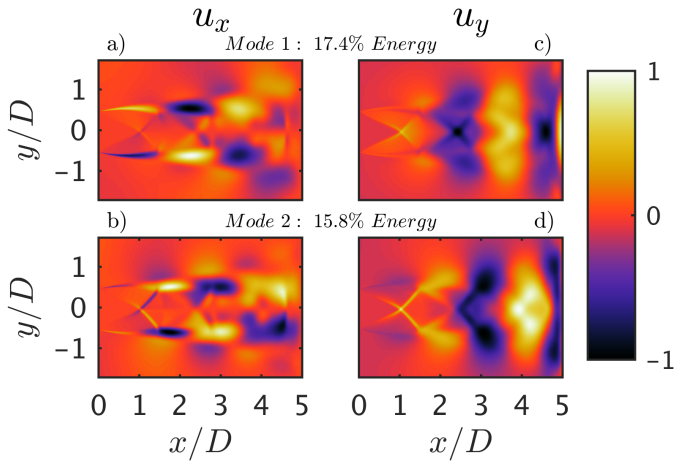

Figure 8: *The two dominant POD modes of the thin lip nozzle case. POD was performed on over 10000 samples.*

their energy content, they appear to be separated into two mode pairs. Figure 9 illustrates these four modes, both axially and transversely. Again, from Figure 9 the first and second mode have a similar structure, but are out of phase. The same thing is true for modes three and four, which confirms the separation of the modes into two pairs. The first and second pair contain 23.4% and 12.2% of the specific energy, respectively. It is noted that the first mode pair is symmetric about the centreline for the axial component and asymmetric for the transverse component. The opposite is true for the second mode pair. This suggests the flow is dominated by a global symmetric mode, with a secondary, asymmetric mode also existing in the flow.

The change of dominant modes between the thin and infinite lip cases highlights a significant difference between these flows. While the asymmetric mode remains in the infinite lip case, its strength is significantly reduced compared to the helical mode of the thin lip flow. The toroidal mode present in the infinite lip condition is not observed in the first 10 modes of the thin lip POD. This suggests that the toroidal mode's existence at this NPR and plate spacing is dependent on the infinite lip nozzle geometry.

Triple Decomposition

To determine if the previously discussed differences in variance for the two cases are related to the dominant global modes, a triple decomposition is applied to the flow. By taking the velocity fluctuations associated with the dominant POD modes to be the coherent component of the flow, the triple decomposition is obtained as per Equation 1. For the thin lip, the coherent component are associated with the first two orthogonal modes. Isolating the fluctuations associated with these modes separates the stochastic flow into its coherent and random components. The variance of each component is then calculated individually. The same method is applied to the infinite lip nozzle flow, however, here the first four modes are found to make up the coherent component.

The transverse variances of the coherent and random components for each nozzle are presented in Figure 11. Figure 11a shows that the high variance located at the shock cells is present in the coherent component of the fluctuations. This corresponds to the dominant global mode of the jet flow. Again, no notable

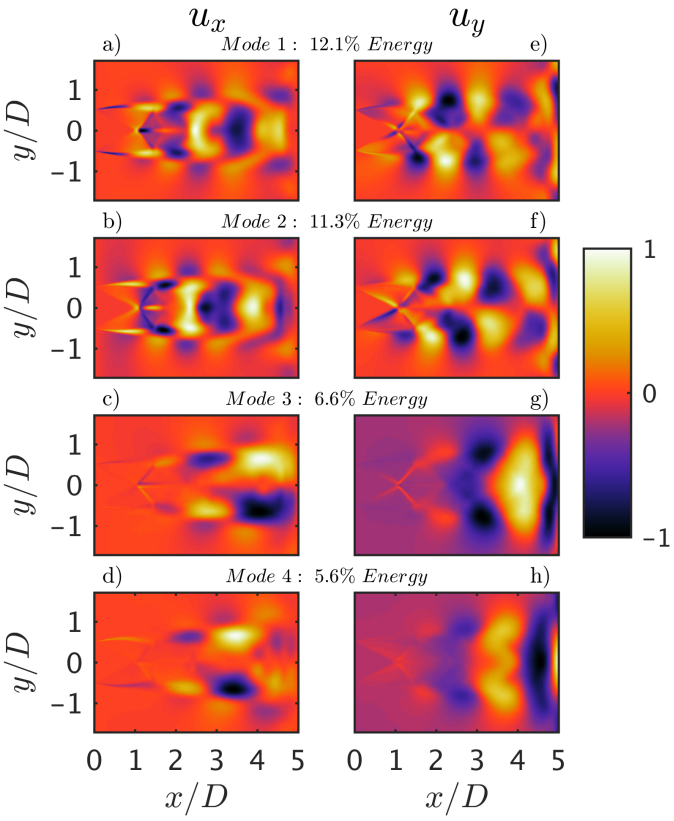

Figure 9: *The first four dominant POD modes of the infinite lip case. POD performed on over 10000 samples.*

high variance is observed along the jet centreline for the infinite lip nozzle for either the coherent or random components. This is not unexpected given the dominant toroidal mode of the infinite lip case. This fluctuation is thus due to the transverse oscillation of the first shock cells, as a consequence of the passing helical mode shear layer vortices.

The axial variances for the fluctuating components for each nozzle are given in Figure 10. Whilst high variance is shown in the random fluctuations of the standoff shock region, the axial thickness is small for both conditions. However, the coherent fluctuations for the infinite lip jet, show a large axial region of high variance. This suggests that the axial oscillation of the standoff shock for the infinite lip case is due to the dominant global mode as suggested previously. There is no axial variance in the coherent component of Figure 10 for the thin lip case, which confirms that the helical mode does not cause axial oscillation of the standoff shock.

Conclusions

The difference between two nozzle geometries was investigated experimentally using PIV. Both jet flows have an NPR of 3.4 and plate spacing of $z/D = 5.0$. First and second order statistics highlight similarities and differences in the overall jet structure of these two configurations. The mean axial and transverse flows of both jets were comparable, with similar shock cell spacing. From the measured variances, a larger shear layer was found for the infinite lip compared to the thin lip jet.

An increase in transverse variance was observed for the thin

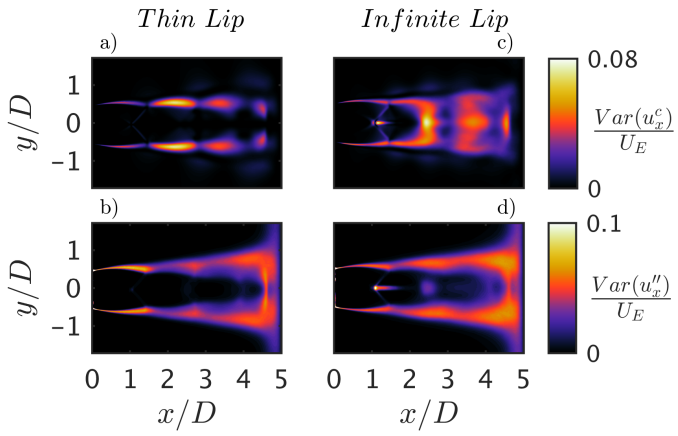

Figure 10: *Axial Variance of the two fluctuating components, coherent and random, for both the thin and infinite lip jet. Variance calculated over 10000 images.*

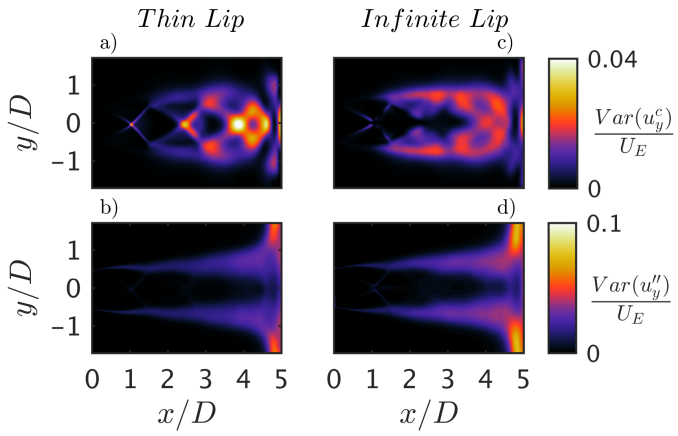

Figure 11: *Transverse Variance of the two fluctuating components, coherent and random, for both the thin and infinite lip jet. Variance calculated over 10000 images.*

lip flow at the shock cell locations and suggesting that it is related to the nature of the dominant mode of the jet. In the axial component, a larger region of high variance is observed for the infinite lip jet, attributed to an oscillation of the standoff shock. It is proposed that this is due to a global symmetric mode. Proper orthogonal decomposition is performed on both flows, highlighting a difference in global modes. The thin lip jet is dominated by a single, helical mode, whereas the infinite lip condition contained two mode pairs. Of these the dominant mode is symmetric, with the secondary mode being asymmetric. By using a triple decomposition of the flow velocity, the increased region of high transverse variance is found to be the result of the dominant global mode of the thin lip jet. This indicates that the transverse oscillation of the early shock cells is due to the global mode. Similarly, a large region of high axial variance at the standoff shock is found in the coherent component of the infinite lip jet. This suggests that the axial oscillation of the standoff shock is indeed due to the global axisymmetric mode. No region of high variance is present in the coherent fluctuations of the thin lip. Thus it is concluded that the global asymmetric mode of the thin lip jet does not induce an axial oscillation of the standoff shock.

Acknowledgements

This research was supported under Australian Research Council's Discovery Projects funding scheme.
This research was undertaken with the assistance of resources provided at the NCI National Facility systems at the Australian National University through the National Computational Merit Allocation Scheme supported by the Australian Government.

References

[1] Andr, B., Castelain, T., and Bailly, C. (2014). *Investigation of the mixing layer of underexpanded supersonic jets by particle image velocimetry*. International Journal of Heat and Fluid Flow, 50, 188-200.

[2] Brown, G. L., and Roshko, A. (1974). *On density effects and large structure in turbulent mixing layers*. Journal of Fluid Mechanics, 64(04), 775-816.

[3] Choi, J. J., Annaswamy, A. M., Lou, H., and Alvi, F. S. (2006). *Active control of supersonic impingement tones using steady and pulsed microjets*. Experiments in fluids, 41(6), 841-855.

[4] Donaldson, C. D., and Snedeker, R. S. (1971). *A study of free jet impingement. Part 1. Mean properties of free and impinging jets*. J. Fluid Mech, 45(2), 281-319.

[5] Edgington-Mitchell, D., Oberleithner, K., Honnery, D. R., and Soria, J. (2014). *Coherent structure and sound production in the helical mode of a screeching axisymmetric jet*. Journal of Fluid Mechanics, 748, 822-847.

[6] Edgington-Mitchell, D., Honnery, D. R., and Soria, J. (2014). *The underexpanded jet Mach disk and its associated shear layer*. Physics of Fluids (1994-present), 26(9), 096101.

[7] Edgington-Mitchell, D., Duke, D., Amili, O., Weightman, J., Honnery, D. R., and Soria, J. (2015). *Measuring shear layer growth rates in aeroacoustically forced axisymmetric supersonic jets*. In 21st AIAA/CEAS Aeroacoustics Conference (p. 2834).

[8] Henderson, L. F. (1966). *Experiments on the impingement of a supersonic jet on a flat plate*. Zeitschrift fr angewandte Mathematik und Physik ZAMP, 17(5), 553-569.

[9] Henderson, B., and Powell, A. (1993). *Experiments concerning tones produced by an axisymmetric choked jet impinging on flat plates*. Journal of Sound and Vibration, 168(2), 307-326.

[10] Henderson, B. (2002). *The connection between sound production and jet structure of the supersonic impinging jet*. The Journal of the Acoustical Society of America, 111(2), 735-747.

[11] Henderson, B., Bridges, J., and Wernet, M. (2005). *An experimental study of the oscillatory flow structure of tone-producing supersonic impinging jets*. Journal of Fluid Mechanics, 542, 115-137.

[12] Ho, C. M., and Nosseir, N. S. (1981). *Dynamics of an impinging jet. Part 1. The feedback phenomenon*. Journal of Fluid Mechanics, 105, 119-142.

[13] Hussain, A. and Reynolds, W., *The mechanics of an organized wave in turbulent shear flow*, J. Fluid Mech., Vol. 41, 1970, pp. 241258.

[14] Krothapalli, A. (1985). *Discrete tones generated by an impinging underexpanded rectangular jet*. AIAA journal, 23(12), 1910-1915.

[15] Krothapalli, A., Rajkuperan, E., Alvi, F., and Lourenco, L. (1999). *Flow field and noise characteristics of a supersonic impinging jet*. Journal of Fluid Mechanics, 392, 155-181.

[16] Kuo, C. Y., and Dowling, A. P. (1996). *Oscillations of a moderately underexpanded choked jet impinging upon a flat plate*. Journal of Fluid Mechanics, 315, 267-291.

[17] Marsh A (1961). *Noise measurements around a subsonic air jet impinging on a plane, rigid surface*. J Acoust Soc Am 33:1065-1066.

[18] Mason-Smith, N., Edgington-Mitchell, D., Buchmann, N. A., Honnery, D. R., and Soria, J. (2015). *Shock structures and instabilities formed in an underexpanded jet impinging on to cylindrical sections*. Shock Waves, 1-12.

[19] Meyer, K., Pedersen, J., and Ozcan, O. (2007). *A turbulent jet in crossflow analysed with proper orthogonal decomposition*, J. Fluid Mech., Vol. 583, pp. 199227.

[20] Mitchell, D. M., Honnery, D. R., and Soria, J. (2012). *The visualization of the acoustic feedback loop in impinging underexpanded supersonic jet flows using ultra-high frame rate schlieren*. Journal of Visualization, 15(4), 333-341.

[21] Papamoschou, D., and Roshko, A. (1988). *The compressible turbulent shear layer: an experimental study*. Journal of Fluid Mechanics, 197, 453-477.

[22] Powell, A. (1988). *The sound producing oscillations of round underexpanded jets impinging on normal plates*. The Journal of the Acoustical Society of America, 83(2), 515-533.

[23] Raman, G. (1997). *Cessation of screech in underexpanded jets*. J. Fluid Mech, Vol. 336, pp. 6990.

[24] Raman, G. (1999). *Supersonic jet screech: half-century from Powell to the present*. Journal of Sound and Vibration, 225(3), 543-571.

[25] Seiner, J. M., and Norum, T. D. (1979). *Experiments on shock associated noise of supersonic jets*. AIAA paper, 1526, 1979.

[26] Sirovich, L. (1987). *Turbulence and the dynamics of coherent structures. I-Coherent structures. II-Symmetries and transforma- tions. III-Dynamics and scaling*, Quarterly of applied mathematics, Vol. 45, pp. 561571.

[27] Soria, J. (1996). *An investigation of the near wake of a circular cylinder using a video-based digital cross-correlation particle image velocimetry technique*. Experimental Thermal and Fluid Science, Vol. 12, pp. 221233.

[28] Tam, C. K., and Ahuja, K. K. (1990). *Theoretical model of discrete tone generation by impinging jets*. Journal of Fluid Mechanics, 214, 67-87.